



Influence of site and tower types on urban natural ventilation performance in high-rise high-density urban environment

Hao Qin^a, Pingying Lin^{b,c,*}, Stephen Siu Yu Lau^d, Dexuan Song^b

^a Department of Architecture, The University of Hong Kong, Hong Kong, China

^b College of Architecture and Urban Planning, Tongji University, No.1239 Siping Road, Shanghai, 200092, China

^c Shanghai Key Laboratory of Urban Renewal and Spatial Optimization Technology, China

^d Department of Architecture, National University of Singapore, 117566, Singapore



ARTICLE INFO

Keywords:

Urban ventilation
High-rise high-density
CFD
Building typology
Site division strategy
Tower type

ABSTRACT

This paper investigates the urban ventilation performance at the street and tower-level in the high-rise high-density urban environment of Hong Kong. By analyzing 218 residential developments and 659 residential towers from 2003 to 2013, this paper presented an innovative way of generating idealized urban forms that considers the regulatory and social-economic factors. Nine typical high-rise high-density residential urban design scenarios with different site division strategies and tower types were generated. The urban ventilation performance of these cases was studied using a validated CFD simulation technique under four different approaching wind directions. Two indices were applied to quantify the urban ventilation performance in this study, namely Wind Velocity Ratio (WVR) and Local Mean Age of Air (MAA). The results show that site and tower types have a great influence on urban ventilation. This paper concludes that extra-large sites (around 4000 square meters) have the potential of achieving the best performance in both street and urban level ventilation, while probably enduring poor indoor air quality. Therefore, a centralized tower plan without deep re-entrants is recommended for large sites. For the small (around 500 square meters) and medium (around 1000 square meters) sites that generally have poor street-level ventilation, adding service lanes can help to improve the street ventilation but may cause poor tower-level ventilation since two rows of towers are closely placed in one street block. For the small sites without service lanes, small and rectangular tower plans in one row could help to achieve better tower-level ventilation and indoor air quality potential.

1. Introduction

Health risks due to air pollution exposure have emerged as a major public health issue. In urban areas, the air pollution issue is critical due to the emissions from the high concentration of human activities. An epidemiological study conducted in Kolkata and Delhi during 2000–2006 observed that, compared with rural residents, people living in the cities had a significantly higher prevalence of upper and lower respiratory symptoms, bronchial asthma, and lung function deficits [1]. In cities like Hong Kong, most of the disease burden has come from non-communicable diseases, with about 10–50% of the causes associated with the living environment [2]. Lin et al. [3] found that exposure to elevated ambient air pollutants, such as NO₂ and SO₂, contributed to the increase of acute myocardial infarction mortality based on the data from 1998 to 2000 in Hong Kong.

Urbanization has largely transformed the natural landscape and urban climate conditions which significantly alters the wind environment. Hong Kong has been regarded as a high-rise high-density city by many researchers [4,5] due to its fast urbanization and limited land supply. Such urban environment is considered problematic in pollutant dispersion. With a compact urban environment and concentrated pollution source from vehicles, Hong Kong is facing serious air quality problems, especially on the roadside. Due to its unique urban environment, the Hong Kong government has released a series of regulations to control the urban form in the past decades. Consequently, the developers, guided by their profit-driven nature [6], have constructed a series of typical urban forms under different generations of regulation as shown in Fig. 1e. This paper aims to investigate the urban ventilation performance of idealized urban forms under current planning regulation using CFD simulation and proposing urban design strategies for Hong

* Corresponding author. College of Architecture and Urban Planning, Tongji University, No.1239 Siping Road, Shanghai, 200092, China.

E-mail address: pingylin@outlook.com (P. Lin).

Kong to achieve better urban ventilation.

Among the methods for studying the influence of built forms on natural ventilation performance, Computational Fluid Dynamics (CFD) has been proved to be cost-effective and has been widely used by many researchers [7–9]. The validity and accuracy of different turbulence models has been thoroughly examined by many researchers [10–12]. The accuracy of various RANS-based turbulence models has been investigated and the result showed that each model has its advantage in certain ventilation problems [13–15]. The modeling techniques throughout the preprocessing, processing and post-processing period have also been widely studied [15–17]. Ramponi and Blocken [18] investigated the impact of computational domain size, the grid resolution, the inlet turbulent kinetic energy profile of the atmospheric boundary layer, the turbulence model, the order of the discretization schemes and the iterative convergence criteria on the simulation accuracy and found out SST $k-\omega$ model has the best ventilation performance.

Franke et al. [19] and Tominaga et al. summarized and proposed various modeling techniques on domain size, boundary condition, meshing, etc. for conducting CFD simulation in the urban environment.

In terms of research objects, the studies on urban ventilation can be divided into two categories based on the way to generate these forms and their complexity:

- Simple generic forms: these studies used single cubic buildings [20], street canyons [21], cubic building groups [22] and cuboid building groups [23] to study the impact of building aspect ratio, street aspect ratio, building density [24], building height variation [25] and building location on the wind flow and pollutant dispersion [26–28].
- Realistic urban settings: with the developments in computer technology, there has been an increasing body of literature studying the urban ventilation in realistic urban settings. These studies investigated various urban settings such as a football stadium with complex

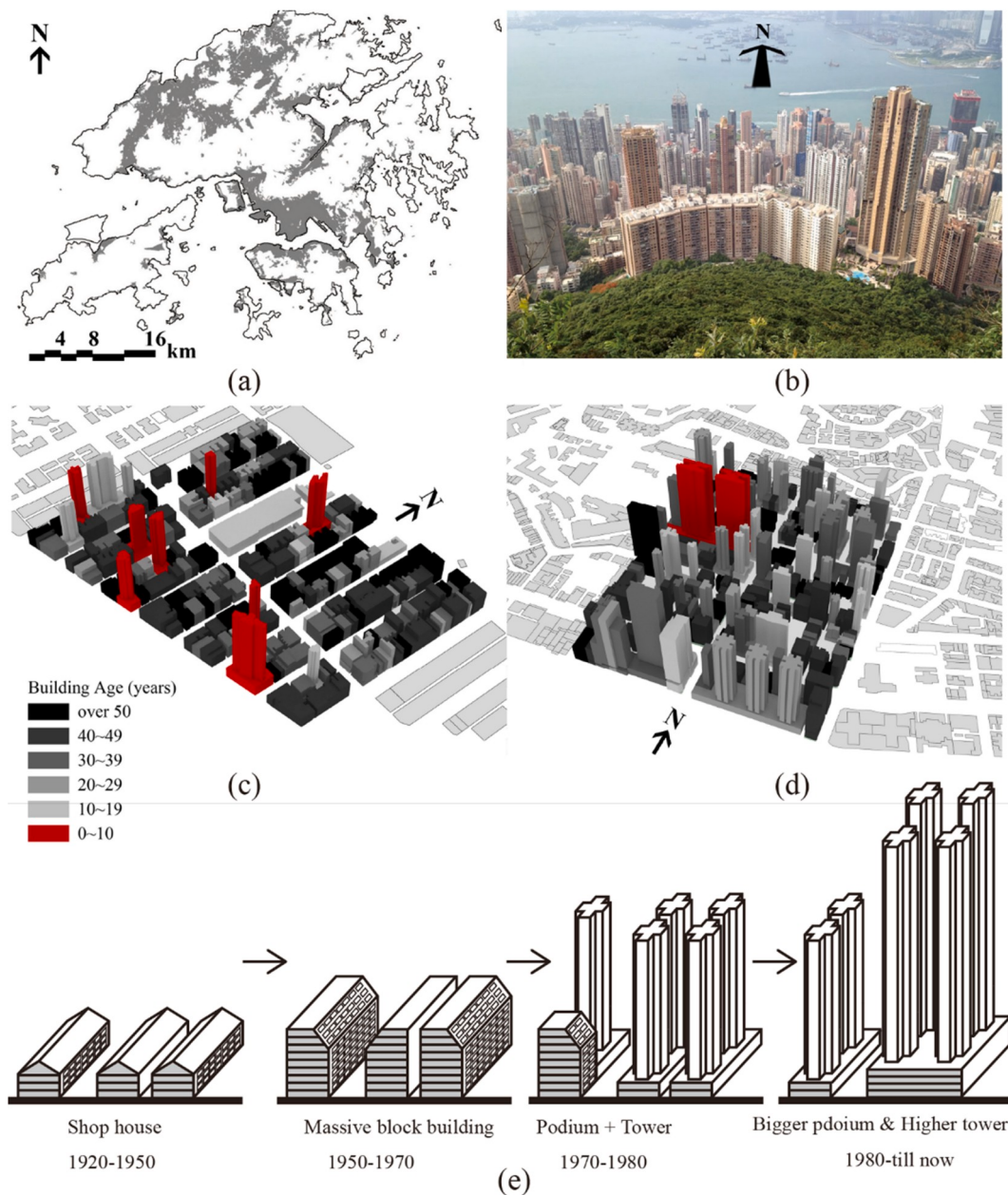


Fig. 1. (a) Built-up area of Hong Kong in grey; (b) Urban environment of Hong Kong (birds-eye-view from the peak of Hong Kong island viewing north); (c) Urban area of Hong Kong in the early phase of urban development (birds-eye-view from southeast direction) and (d) later phase of urban development (birds-eye-view from southeast direction); (e) typical building forms built under the different generations of regulation.

surrounding buildings [29], low-rise high-density urban areas [30], university campus [31].

It can be seen from literature that most of the generic urban forms are simple cuboids that are only useful in studying parameters such as aspect ratio, density, height variation and etc. While the realistic urban settings are confined to the certain urban environment and particular urban ventilation problems. There is a gap of research object between generic forms and realistic urban settings. A few researchers have been starting to study urban forms considering the unique urban environment. Yuan and Ng [32] examined the ventilation conditions of parametric building clusters generated from Hong Kong's urban grid. He et al. [33] studied the impact of angular road patterns on urban ventilation using high-density urban settings generated from Singapore experience. However, very few urban forms are generated according to urban design and architectural principles which consider the urban context, local regulation, social-economic preference.

This paper proposed an innovative way for studying the urban ventilation problem by: first, fully understand the historical urban development, building (planning) regulation, social-economic preference of the city; second, extract the key urban design parameters such as street grid, site type, building type, and building orientation; third, generate the idealized urban forms that represent the extreme condition of particular land division strategy within the typical street grid; fourth, compared the urban ventilation performance of these urban forms using CFD simulation and thus to provide urban design suggestions that can be directly implemented by architects and urban planners.

The abundant urban ventilation studies using CFD technology have proved that it is a valid tool in this research area. The High-rise high-density urban environment of Hong Kong was selected as the study area. The rest of this paper is structured as follows: Section 2 introduces the way to generate urban forms and their typological characters. Section 3 describes the CFD simulation settings. Section 4 shows the validation of CFD results with the wind tunnel data. Results and discussion are presented in Section 5 and conclusions are drawn in Section 6.

2. Generation of urban forms

Before conducting CFD simulation, the history of residential development in Hong Kong was analyzed. Plans and configurations of high-rise private residential developments all over Hong Kong (except for a few developments in Lantau Island) from 2003 to 2013 were collected from <http://hk.centamap.com/>, a website run by Centaline Property Agency. A total of 218 private residential developments (659 towers) from this period were investigated. To generate realistic urban design scenarios that reflect the typical tower types in Hong Kong, the following aspects were considered: ① urban design features such as street grids, site types and tower types; ② building regulations and urban design principles; ③ the profit-driven nature of developers and their influence on the residential building designs. Based on the above analysis, a series of urban forms were generated and tested using well-validated CFD models with justified evaluation indices such as air change rate and mean age of air.

2.1. Urban development of Hong Kong

Hong Kong is located on the southeast coast of China with a land area of 1104 km², most of which is mountainous [34]. Due to its unique geological condition, only less than 30% of the land is the built-up area (Fig. 1a) [35]. Among the whole urban area, only 76 km² is the residential area (including 35 km² of rural development). Meanwhile, the population of Hong Kong has grown from less than 2 million to more than 7 million over the last 70 years [36]. To accommodate such a large population with limited land, the building (planning) regulation of Hong Kong has changed through the time which gives birth to different generations of building forms as shown in Fig. 1e. In each period, the

developers of the time tried to build as many areas as they were allowed and tended to choose the building types that were preferred by the buyers. Overtime, Hong Kong has developed into the partial high-rise high-density urban environment [37] as shown in Fig. 1b.

Currently, Hong Kong is regulated under the Building (Planning) Regulations 2012 [38] that allows full coverage of site for buildings under 15 m and plot ratio limit from 8 to 10 for different site types. This regulation has created cake-like building types that are composed of podium and towers. These building types have been gradually transforming the urban area of Hong Kong. Fig. 1c shows the area located in Kowloon of Hong Kong that is still in the early phase of such transformation, while Fig. 1d shows an area located in Hong Kong Island that has already arrived at the later phase of the transformation. It can be found that for the site in the early phase of such transformation, buildings constructed in the recent ten years are all high-rise buildings. Apparently low/mid-rise buildings have been gradually replaced by high-rise buildings during the urban renovation. It is foreseeable that Hong Kong will eventually develop into a complete high-rise high-density urban environment given the current regulations.

2.2. Street grid, site type and corresponding building types of Hong Kong

The street grid is the fundamental urban design factor that affects the urban form [39]. As a post-colonial city, Hong Kong adopted a European street grid system [40]. Typical street grids in Old Town and New Town of Hong Kong can be extracted based on the analysis of the street structure. A clear rectangular street grid arrangement can be found in many of the Old Towns in Hong Kong (Fig. 2a). The length of street blocks ranges from 80 to 160 m and the width ranges from 30 to 50 m. Street width ranges from 8 to 20 m, with the majority being 15 m. Street blocks are usually subdivided by one or more service lanes that create diverse urban fabric and building types [38]. Typically, there is at least one service lane inside the street block that divides the block into two parts. Each part can be further divided into small sites. For the New Town area, a similar street grid system is adopted. But in order to accommodate high-rise buildings with a larger footprint, the service lane is eliminated.

The street grid can be further divided into small sites. According to the Building (Planning) Regulations [38], sites in Hong Kong are classified into three categories with different plot ratio limit as follows (Fig. 2b):

- Class A site means a site, not being a class B site or class C site, that abuts only one specified street wider than 4.5 m; it has a plot ratio limit at 8; considering the GFA concession (a unique regulation in Hong Kong that allows the developer to build up to 10% more plot ratio if certain green features have been implemented), the plot ratio limit is between 8 and 8.8;
- Class B site means a corner site that abuts two specified streets wider than 4.5 m; it has a plot ratio limit between 9 and 9.9;
- Class C site means a corner site that abuts three specified streets wider than 4.5 m; it has a plot ratio limit between 10 and 11;

By studying the site division of residential developments in Hong Kong in the recent 10 years, two more types of sites with different spatial character were identified by the author as follows:

- Class A' site means a site, similar to site A, not being a corner site, that abuts two parallel streets wider than 4.5 m on each side of the site; it also has a plot ratio limit between 8 and 8.8;
- Class D site means a site that is surrounded by four specified streets wider than 4.5 m; for the large site like Class D, it normally located in Kowloon and Kowloon that has a different plot ratio limit between 7.5 and 8.25 [41];

Based on the analysis of 10 years of residential development, the

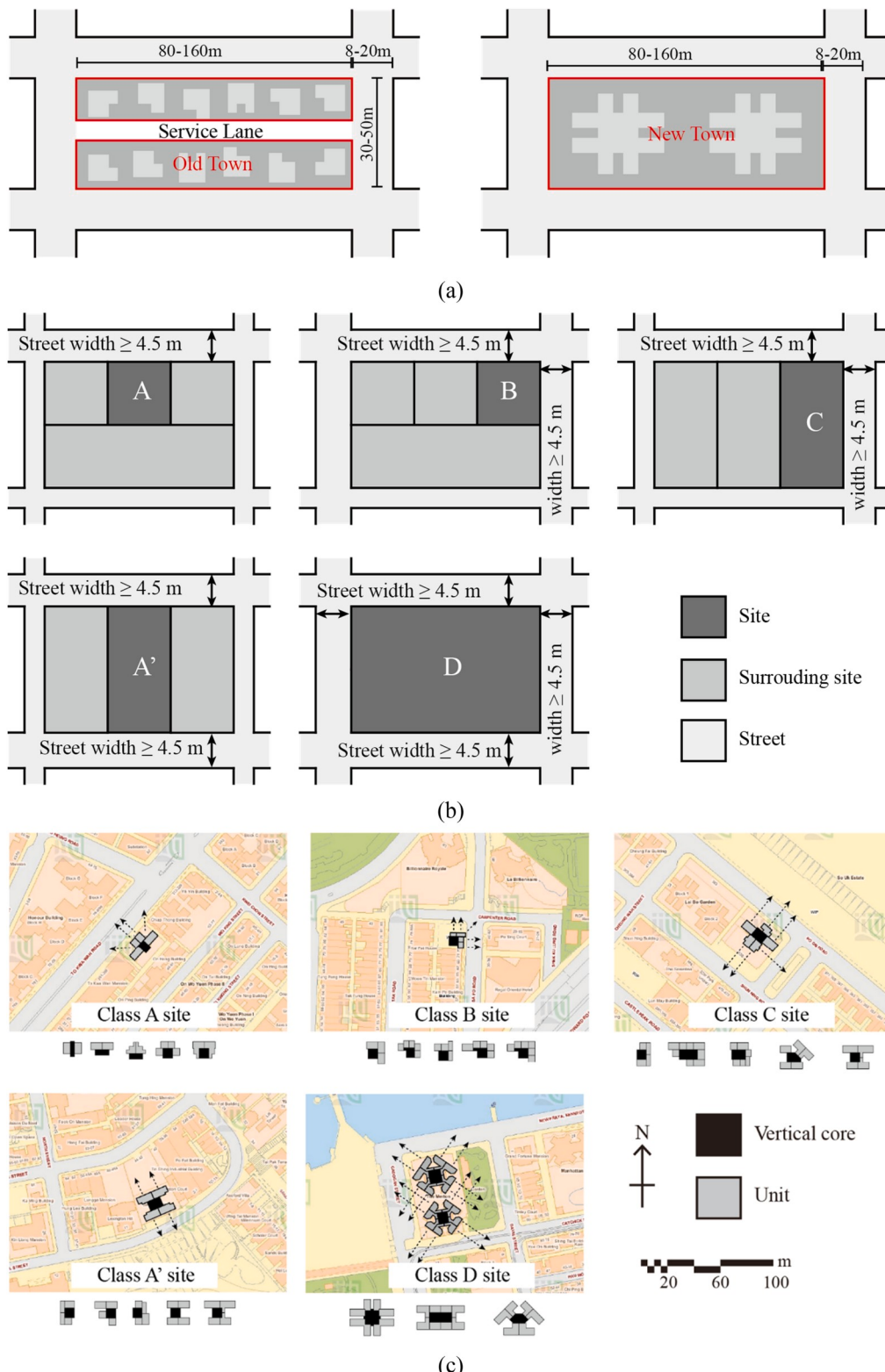


Fig. 2. (a) Typical street grid for residential towers in the metropolitan area of Hong Kong; (b) Site types of Hong Kong after Building (Planning) Regulations [38]; (c) Site types and their corresponding tower types and orientation (base map from <https://www.map.gov.hk>).

strong correlation between site types and the tower types was found. Such correlation can be named as the “view optimization principle” which has a great impact on the value of the housing price [42]. With the crowded surrounding urban environment, each site type only has a better view facing the street(s) they abut. Since the view condition highly affects the value of housing properties in Hong Kong, real estate

developers normally prefer certain plan types with optimized view directions that suit the site types. Fig. 2c shows the site types and their corresponding tower types and orientations based on the analysis. For the Class A site that abuts only one street, towers that maximize the width along the street to fully utilize the view facing the street are preferable. Similarly, for the Class B site, towers that have an “L” shaped

unit arrangement along the street are preferred. For the Class C site, towers with units placed around the core follow "U" shape are widely adopted. Since Class A' site has two abutting streets parallel to each other, the "H" shaped floor plan is normally used. With four side views, Class D site is suitable for the towers with units enclose the core, which usually has a larger footprint.

2.3. Urban design scenarios generated for CFD simulation

Based on the above analysis, we can then generate idealized urban design scenarios under current regulation within the extracted street grid and site divisions in consideration of social-economic preference. In this study, 9 cases with different site area and tower types are generated:

- Firstly, the street block was divided into small sites that fell into four area groups, 500, 1000, 2000 and 4000 square meters. Two different division strategies were applied for the site area of 500, 1000 and 2000 square meters. One with a 3-m wide service lane cut through the central axis along the longer span, which generates cases such as S_{500a}, S_{1000a}, and S_{2000a}. Such service lane must be provided as the routes for access and egress [43] for the class A sites in the middle of the street block, as required by the Building (Planning) Regulation of Hong Kong [38]. Another division strategy generates sites without service lanes, such as S_{500b}, S_{1000b}, S_{2000b}, and S₄₀₀₀. A total of seven site division scenarios can be generated as shown in Fig. 3;
- Secondly, the site plot ratio limit based on the Building (Planning) Regulation of Hong Kong was applied to each site type. The plot ratio varies among site types but is generally similar for each case. Detailed information about each case can be found in Table 1. The slight variation of plot ratio is caused by the particular corresponding tower types;
- Thirdly, corresponding tower types numbered from T1 to T11 were chosen for different site division scenarios. Small sites such as S_{500a} and S_{500b} are correlated to towers with small floor plans such as T1, T2, and T3, while medium sites such as S_{1000a}, S_{1000b} and S_{2000a} are correlated to towers with medium plans such as T4, T5, T6, and T7, large sites such as S₄₀₀₀ and medium site plan with the low aspect ratio as S_{2000b} are correlated to tower with large plans such as T9,

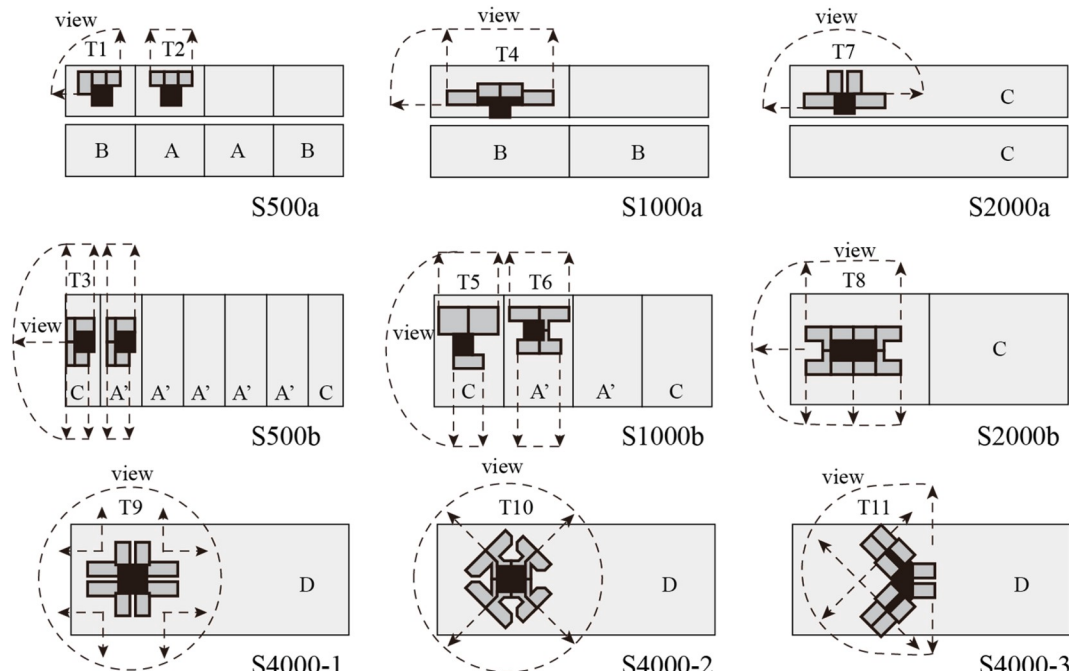


Fig. 3. Street block division and corresponding tower types studied.

Table 1
Characteristics of the study cases.

| Street blocks | Site | Site plot ratio | Case plot ratio |
|---------------------------|------------|-----------------|-----------------|
| S_{500a} | 4 Class A | 8.6 | 9.1 |
| | 4 Class B | 9.6 | |
| S_{500b} | 5 Class A' | 8.5 | 9.0 |
| | 2 Class C | 10.24 | |
| S_{1000a} | 4 Class B | 9.0 | 9.0 |
| | 2 Class A' | 8.1 | 9.2 |
| S_{1000b} | 2 Class C | 10.4 | |
| | | | |
| S_{2000a} | 2 Class C | 8.8 | 8.8 |
| S_{2000b} | 2 Class C | 8.8 | 8.8 |
| S₄₀₀₀₋₁ | 1 Class D | 7.7 | 7.7 |
| S₄₀₀₀₋₂ | 1 Class D | 8.2 | 8.2 |
| S₄₀₀₀₋₃ | 1 Class D | 8.0 | 8.0 |

T10, T11 and T8 based on the "view optimization principle" as shown in Figs. 2 and 3. By following these principles, we can generate 9 different high-rise high-density urban scenarios. All the cases have one vertical street and three horizontal streets that are 15 m wide (Fig. 4a). Since the Hong Kong Building (Planning) regulation allows full site coverage of buildings lower than 15 m for the sites smaller than 20,000 square meters, all the sites were modeled with a 15 m high podium which were widely adopted in Hong Kong to accommodate various space including shops, clinics, kindergartens, restaurants, etc. The tower height was set as 32 stories (96 m) which equals the median value of the 659 towers studied (Fig. 4b).

3. Methodology

CFD technology was used in this study to simulate the ventilation performance of these high-rise high-density urban scenarios. The simulation was conducted using FLUENT 6.3 following the guidelines provided by Franke et al. [19,44] and Tominaga et al. [45].

3.1. Computational domain

The computational domain (Fig. 5a) was modeled based on the guidelines mentioned above. The distance from the inlet to the tested

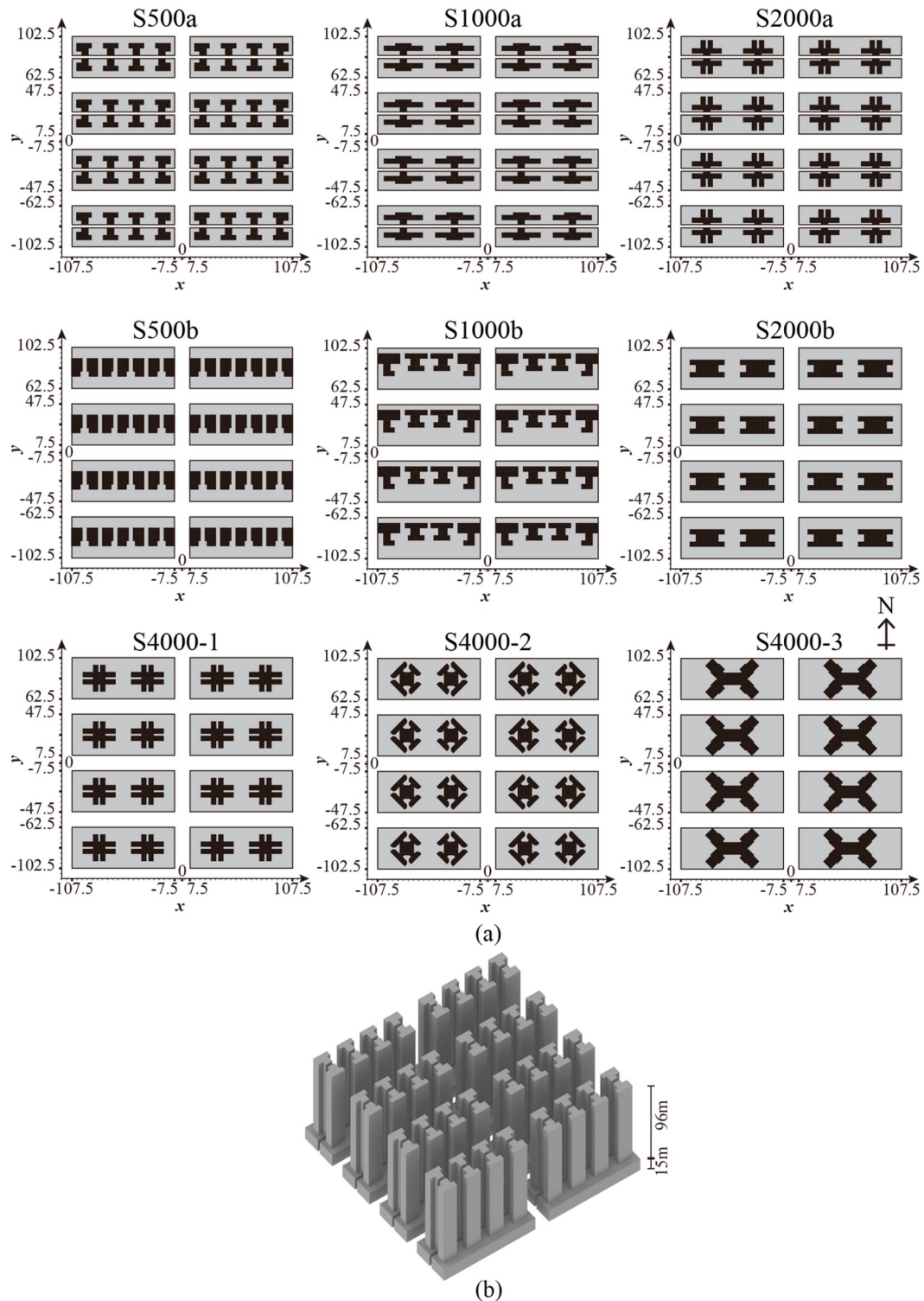


Fig. 4. Illustration of urban design scenario of all study cases.

urban area was set to $5H$ (5 times of building height) and the outlet was $15H$ away from the built area. The height of the computational domain was set to $6H$. Since H was 111 m in this study, the resulting domain size was $2435 \times 2435 \times 666$ m 3 . The blockage ratio was around 1.5%, smaller than the 3% limit required by Franke et al. [19]. Four wind directions, namely West (W, 0°), West-southwest (WSW, 22.5°), Southwest (SW, 45°) and South-southwest (SSW, 67.5°) were calculated. As suggested by the Air Ventilation Assessment Guideline of Hong Kong [46], 16 incoming wind directions with the step of 22.5° should be

conducted for ventilation study in Hong Kong. Since cases in this study adopt a symmetrical layout, these four directions conducted can cover most of the incoming wind conditions.

3.2. Boundary conditions

Since the studied building clusters were presumed to be in the urban area, the wind profile from the experimental site wind availability study for Mong Kok, Hong Kong [47] was referenced. A power-law exponent

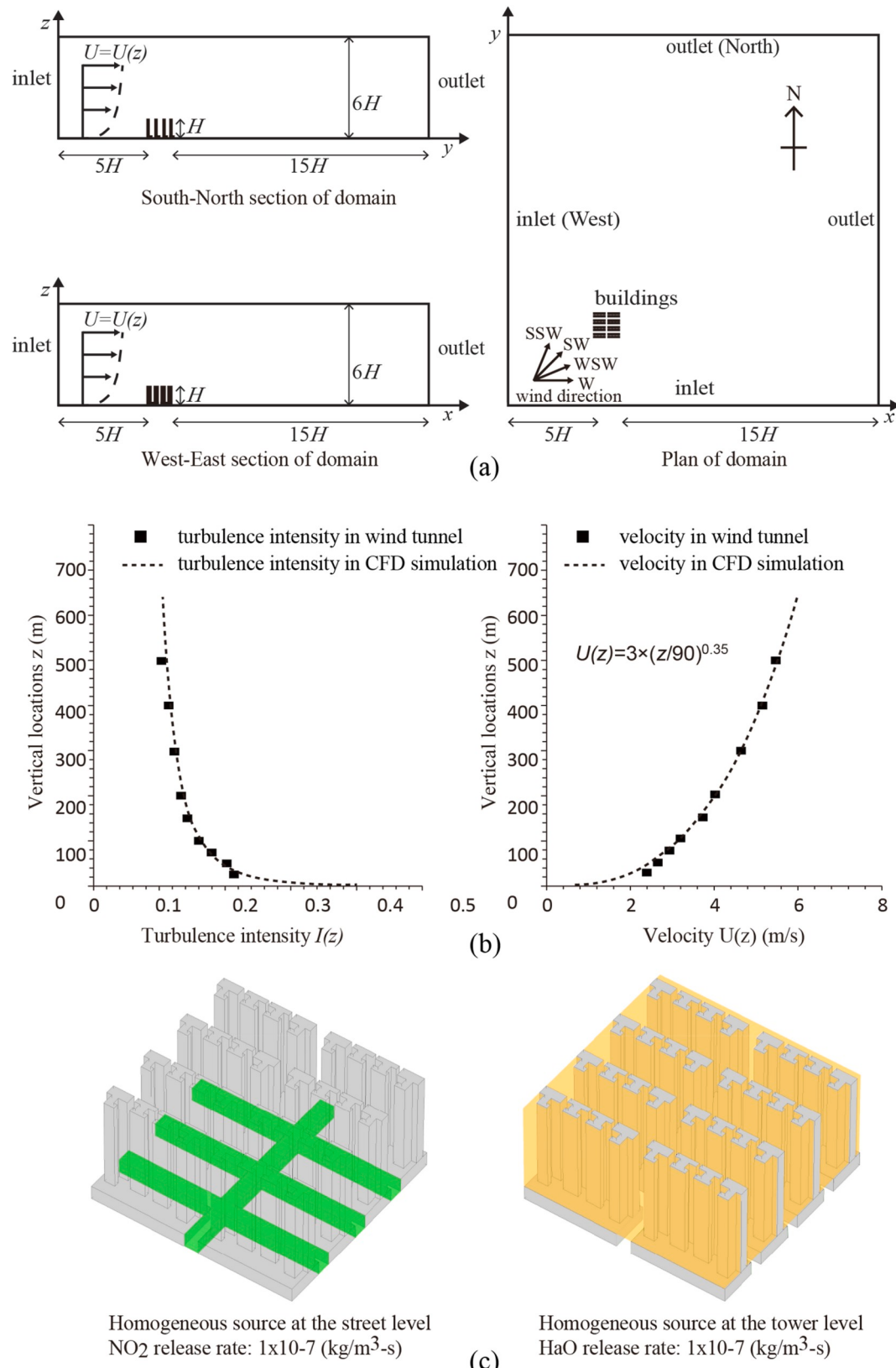


Fig. 5. (a) Dimension of the computational domain; (b) Inlet boundary condition; (c) Homogeneous source at the street-level and tower-level.

of 0.35 was adopted for the inlet boundary conditions for urban area with a heavy concentration of tall buildings [48]. Annual average wind velocity (3 m/s) from King's Park weather station located in the urban area was used as a reference wind velocity. The wind meter of King's

Park weather station is located at 90 mPD (meters above Principle Datum). Therefore, the wind can be calculated through the power law equation below:

$$U_z = 3 \left(\frac{z}{90} \right)^{0.35} \quad (1)$$

The vertical distribution of turbulent kinetic energy (k) and dissipation rate (ϵ) of the inlet boundary were calculated according to the following equations [49]:

$$k = a(Iu)^2 \quad (2)$$

$$\epsilon = C_\mu^{3/4} k^{3/2} / l \quad (3)$$

$$\omega = \epsilon / C_\mu / k \quad (4)$$

where l is the turbulent characteristic length scale which can be approximated as $l = 0.07L$. L is the inlet duct height. C_μ and a were set as a constant value of 0.09 and 1.5 respectively. Zero static pressure boundary conditions were applied to the outlet. No-slip wall boundary conditions were adopted at the top, ground and building wall surfaces of the domain.

The incoming velocity and turbulence intensity profile are shown in Fig. 5b.

3.3. Indices of ventilation performance

Two indices were applied to quantify the urban ventilation performance in this study, namely Wind Velocity Ratio (WVR) and Local Mean Age of Air (MAA). WVR indicates the pedestrian wind availability of urban area which can be calculated using the following equation as suggested by the technical circular for applying air ventilation assessments in Hong Kong [46]:

$$WVR = \frac{V_p}{V_\infty} \quad (5)$$

where V_p is the wind velocity at pedestrian level (1.5 m above the ground) inside the urban area;

V_∞ is the reference wind velocity, which captures the wind velocity at the top of the wind boundary layer (typically assumed to be around 400 m–600 m above city center), while in this paper, reference wind velocity of 5.47 m/s at 500 m above the city center according to equation (1) was used [46];

The homogeneous emission method proposed by Hang and Li [50] was used to calculate the MAA in the urban area. Two different materials were released. For street canyon, NO₂ as the main pollutant source from the vehicles was released inside the whole street canyon with a volumetric rate of 1x-07 kg m⁻³ s⁻¹, same to the value suggested by Hang and Li [50]. In the area above the street canyon and under the urban canopy layer (UCL), H₂O was released with a volumetric rate of 1x-07 kg m⁻³ s⁻¹ as well (Fig. 5c). The age of air can be calculated using the following equation:

$$Age = \frac{C(t)}{S} \quad (6)$$

where,

Age is the nominal age of air (s);

$C(t)$ is the concentration of pollutant as a function of time;

S is the homogenous pollutant release rate in the urban area, which is 1x-07 kg m⁻³ s⁻¹ in this study.

Based on equation (6), we can then calculate the volumetric mean age of air (MAA) at street-level (whole street canyon) and tower-level (the area from 15 m to 111 m above the ground). The area of the street-level and tower-level are illustrated in Fig. 5c.

3.4. Grid resolution

The structured mesh was applied to the whole domain for all the cases. Fig. 6 shows the axonometric view of all the cases with surface grids. A minimum mesh size of 0.4 m was applied to the mesh near the ground, at the building corner and the building top to fully capture the geometrical character of each case. Coarser meshes were adopted for the cells away from the building surface. The maximum stretching ratio of 1.3 as required by Tominaga et al. [45] was adopted to control the growth of the grid size between two consecutive cells. The overall grid size for case S_{500a}, S_{500b}, S_{1000a}, S_{1000b}, S_{2000a}, S_{2000b}, S₄₀₀₀₋₁, S₄₀₀₀₋₂ and S₄₀₀₀₋₃ as 7.7 million, 6.1 million, 7.6 million, 6.8 million, 6.7 million, 4.8 million, 6.8 million, 10.2 million and 12.4 million respectively. The difference in cell size was due to the different building geometry in each case.

3.5. Solver settings

This study used the FLUENT 6.3 to solve the steady-state isothermal turbulence flow with the RANS-based turbulence model with double precision. The selection of turbulence model was based on the sensitivity analysis conducted among 6 RANS-based models, namely Standard $k-\epsilon$ model (SKE) [51], Realizable $k-\epsilon$ model (RKE) [52], Re-Normalization Group $k-\epsilon$ model (RNG) [53], Standard $k-\omega$ model (SKW) [54], Shear stress transport $k-\omega$ model (SST) [55] and Reynolds Stress Model (RSM) [56]. The Shear stress transport $k-\omega$ (SST) model was found most accurate, the validation will be described in Section 3.3. The SIMPLE algorithm was applied for pressure-velocity coupling. Second-order discretization schemes were used for all terms in the transport equations. The simulation was assumed to reach convergence when the residual for continuity was below 10^{-4} , the residuals for k, ω and x, y, z momentum were below 10^{-5} .

4. Validation of CFD results

4.1. Description of wind tunnel experiment

To validate the CFD model, this study utilized the wind tunnel data of the near field pollutant dispersion experiment of a building array that conducted by Tominaga and Stathopoulos [57] to compare with the CFD result. The experiment was carried out in a 13 m long boundary layer wind tunnel with a test section of 1.8 × 1.8 m at Niigata Institute of Technology. As the pollutant source, Ethylene (C₂H₄) was released as a point source in the middle of a street canyon at the ground level. The concentration of the pollutants was 1000 ppm with a vertical velocity (u_z) of 0.456 m/s, which was measured using a high-speed total Hydro-Carbon Analyzer. The statistical concentration values were averaged for 30 s. In the experiment, a building array with 5 × 6 buildings was placed around the pollutant source to represent the urban context. The building blocks were cuboids with the same dimension of width and height (H), and the length being $2H$. The street width was also H as shown in Fig. 7a. A detailed description of the wind tunnel and experiment can be found from Tominaga and Stathopoulos [9,57].

4.2. Computational domain and boundary condition

All 30 building blocks as described in the wind tunnel experiment were modeled in the computational domain. The distances between the building array and the inlet, outlet and lateral boundaries were set as 15H (Fig. 7a). The total computational domain covers a volume of 41H (x) × 44H (y) × 10H (z). The blockage ratio of the domain was 2.3%, lower than the 3% limit. The inlet boundary conditions of the CFD simulation were applied based on the data of wind tunnel measurement. The power-law exponent of incoming vertical wind profile was 0.21 with a reference wind velocity (u_b) of 3.8 m/s at the building height (H). The turbulence intensity of the inlet was 20% at the building height

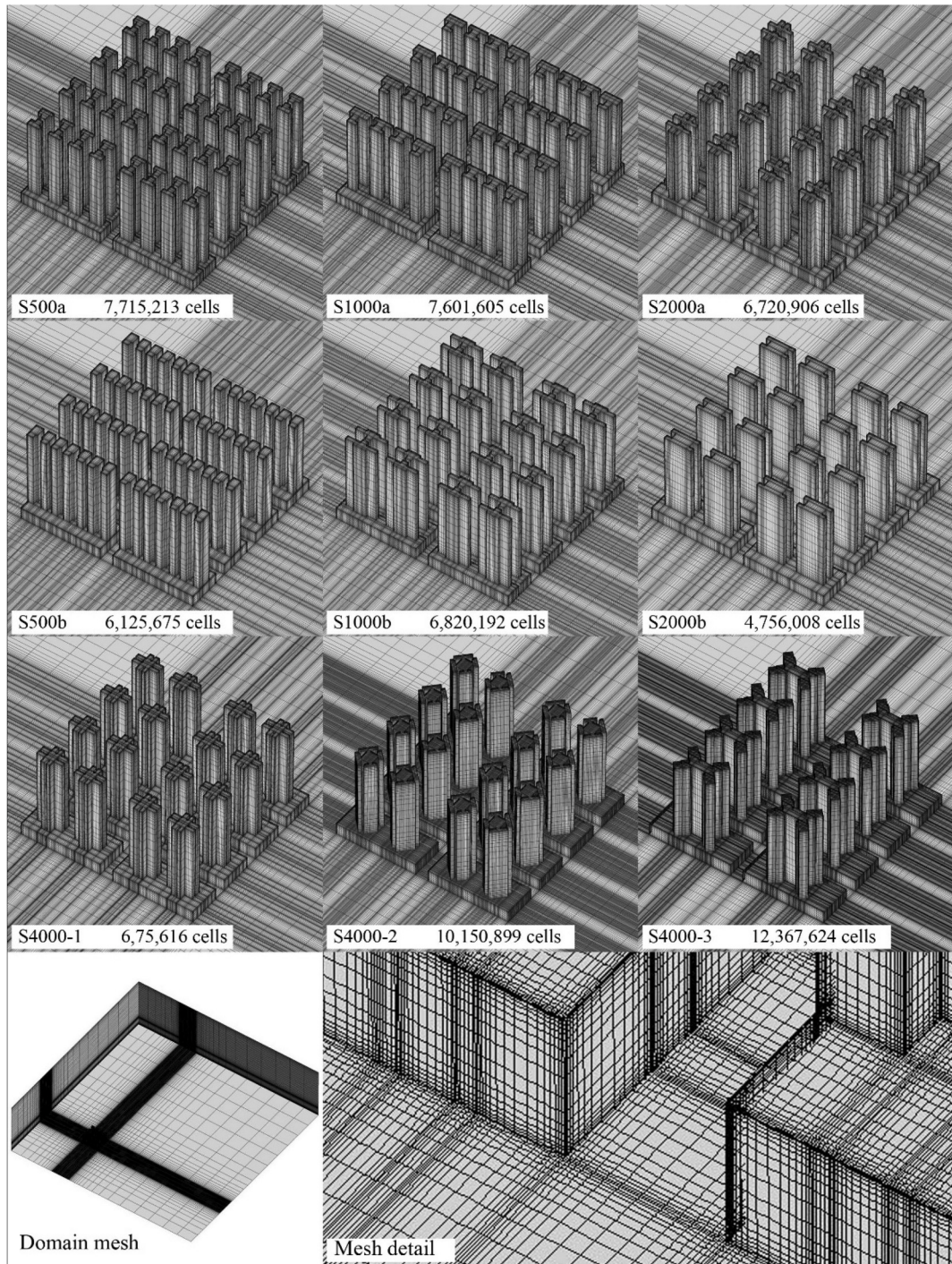


Fig. 6. Axonometric view of the mesh in the domain area and all the cases.

(Fig. 7b).

$$u_z = u_b(z/H)^{0.21} \quad (7)$$

The turbulent kinetic energy k was calculated as follows, where $a = 1$ was used:

$$k = a(I\bar{u})^2 \quad (8)$$

Based on the result of the turbulence model selection, only the Shear stress transport $k-\omega$ model (SST) was used in this simulation; ω was calculated using the following equation:

$$\omega = \frac{C_\mu^{-1/4} k^{1/2}}{l} \quad (9)$$

where $C_\mu = 0.09$,

$l = 0.07L$ and L equals to the height of the computation domain (10 m).

The pollutant inlet was set up as a square shape inlet with a size of $0.1H \times 0.1H$, the same as the size described by Tominaga and Stathopoulos [57]. The location, velocity, tracer gas, and concentration were

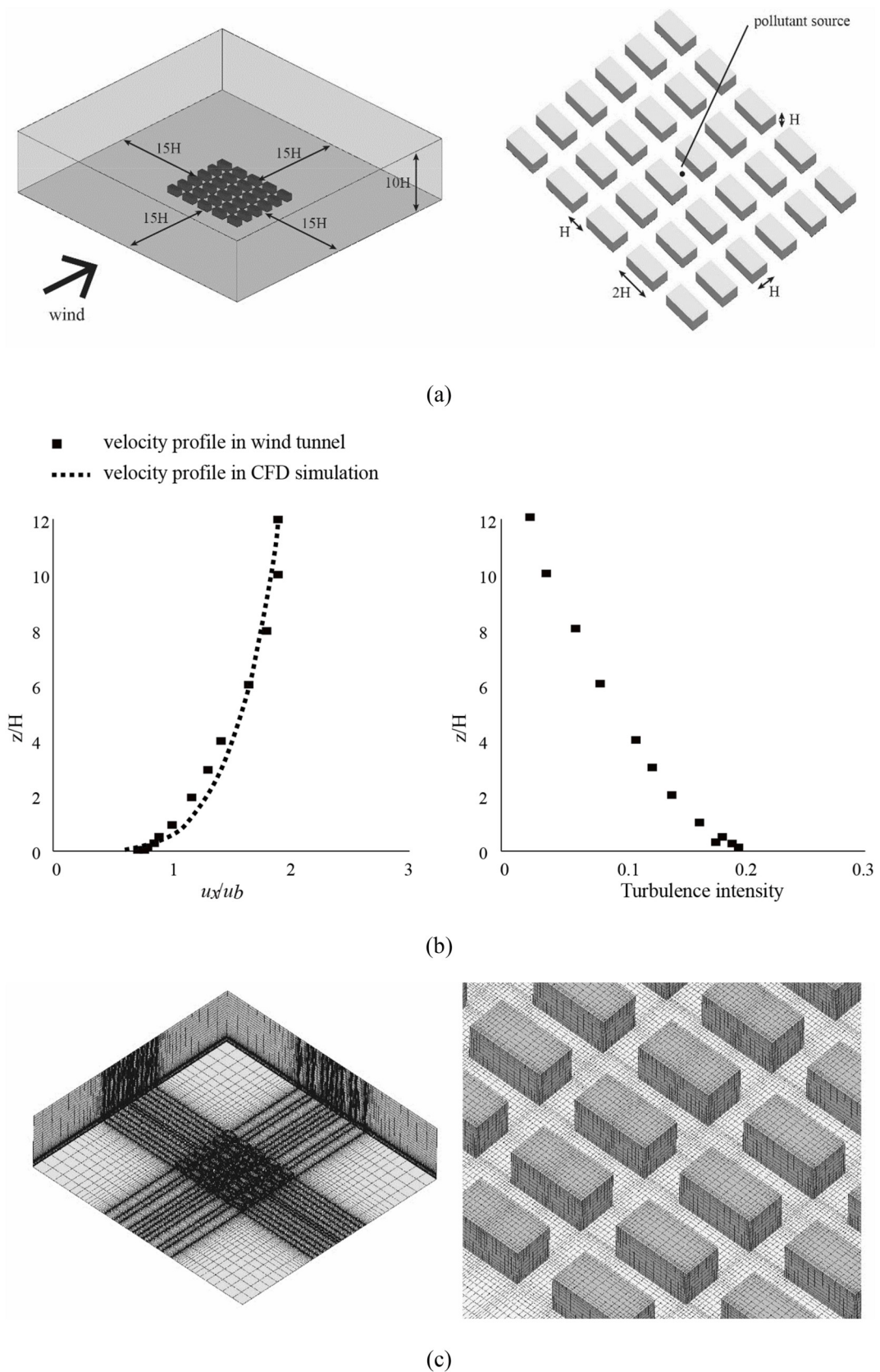


Fig. 7. (a) Computational domain size (left) and building array dimension (right); (b) Inlet boundary condition in the wind tunnel measurement and CFD simulation; (c) Surface grid of the domain (left) and building block (right).

set based on the description of the wind tunnel experiment. Structured meshes were generated using the method suggested by van Hooff and Blocken [58]. A minimum length of $0.05H$ was applied to the pollutant inlet and building boundaries with an expansion ratio of 1.3 to gradually coarsen the cells away from the building array.

The SIMPLE algorithm was applied for pressure-velocity coupling. Second-order discretization schemes were used for all terms in the transport equations. The simulation was assumed to reach convergence when all the scaled residuals became constant in the simulation. Generally, the residual for continuity and C_2H_4 were below 10^{-3} , k and ω were below 10^{-4} , and the residuals for x , y , and z momentum were below 10^{-5} .

As suggested by Tominaga and Stathopoulos [57], the local concentration of C_2H_4 was non-dimensionalized by dividing the reference concentration c_0 :

$$c_0 = \frac{Q_e}{H^2 u_b} \quad (10)$$

where Q_e is the pollutant exhaust rate of the pollutant inlet; H is the building height; and u_b is the reference velocity.

4.3. Validation result

Six different RANS-based turbulence models mentioned in Section 3.5 are applied in each simulation. The results are presented in Fig. 8 and compared with the wind tunnel and LES simulation results from the study by Tominaga and Stathopoulos [57]. It can be seen that both stream-wise (u_x) wind velocity ratio and pollutant concentration inside the street canyon of 6 RANS-based simulation matches well with the wind tunnel experiment and LES simulation. In terms of wind velocity ratio, SST has the average standard deviation error of 0.21, same as RKE and RNG, smaller than SKE, SKW, and RSM. While for pollutant concentration along the vertical centerline, SST has the smallest average standard deviation error of 0.008 among 6 turbulence models. It can be seen from Fig. 8b that the pollutant concentration pattern inside the street canyon in SST simulation is most similar to the experiment. Therefore, the SST model is used in this study.

4.4. Grid sensitivity analysis

As mentioned above, the minimum mesh size of 0.4 m was applied to the mesh near the ground, at the building corner and the building top to fully capture the geometrical character of each case. To ensure the change in mesh detail will not affect the simulation result, a grid sensitivity analysis has been conducted. Three different grids are used to analyze the impact of grid resolution on the simulation results. The fine case has 12,843,492 grids with minimum mesh size down to 0.2 m, the medium case (preferred) has 6,125,675 grids with minimum mesh size down to 0.4 m and the coarse case has 2,748,384 with minimum mesh size down to 0.8 m as shown in Fig. 9a. The same boundary condition and solver settings were applied for three cases and the wind velocity and pollutant concentration along the line $x = 0$ and $y = 0$ at 1.5 m above ground are compared among three cases. The following equation is used to calculate the error rate:

$$\sum \sqrt{\left(\frac{V_0 - V_x}{V_0}\right)^2} / N \quad (11)$$

Where V_0 is the value of fine mesh, V_x is the value of medium or coarse mesh, N is the number of points on line $x = 0$ and $y = 0$;

It can be seen from Fig. 9 that the difference between the medium and fine mesh is trivial, while a large discrepancy is found between the coarse and fine mesh. The error rate of NO_2 concentration is 0.19% and 4.96% for medium and coarse mesh along the line $x = 0$. It shows that using the medium grid with a minimum mesh size of 0.4 m is

appropriate in this work.

4.5. Stream-wise inconsistency test

Stream-wise inconsistency was checked in an empty computation with similar mesh as suggested by Blocken et al. [59,60]. Fig. 10 compares the inlet profiles ($x = -555$), case profile ($x = 0$) and downstream profiles ($x = 1000$). It is observed that the overall profile of wind velocity (u), turbulent kinetic energy (k) and turbulence dissipation rate (ω) at inlet, $x = 0$ and $x = 1000$ agreed well. The acceleration of flow near the ground was observed from the lowest 50 m profile as reported by other researchers [59,61]. The discrepancy was minimized by correlating the sandgrain roughness (ks) with the aero dynamic length (y_0). The small inhomogeneity errors were considered acceptable for the purpose of this research.

5. Result and discussion

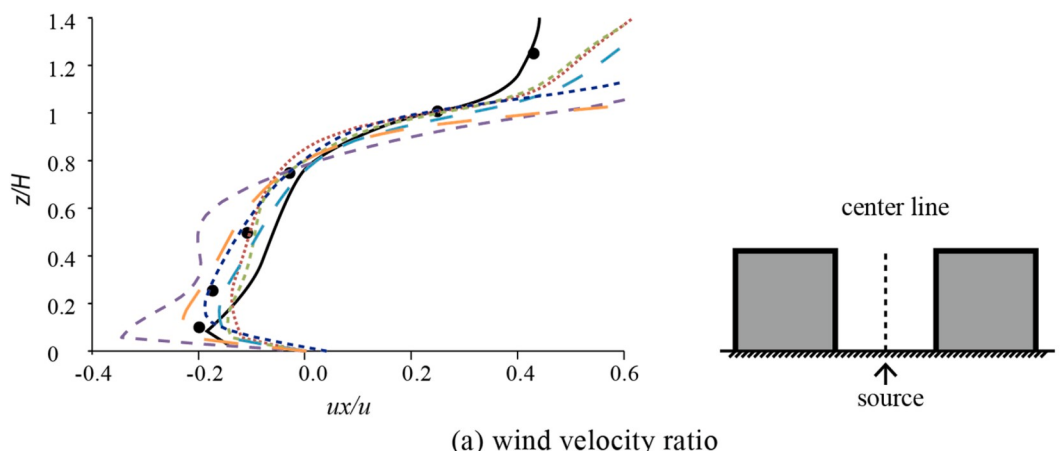
5.1. Ventilation performance at the street-level

Ventilation performance at the street-level concerns the WVR and MAA inside the whole street canyon. The distribution of age of air at 1.5 m above the ground and the volumetric average WVR and MAA of each case under four wind directions are summarized in Fig. 11. The best urban ventilation performance can be achieved when the wind blowing parallel to the street, W wind in this case. On average, the WVR of all 9 cases is 0.46 under W wind, 0.31 under WSW wind, 0.24 under SW wind and 0.20 under SSW wind. There is 31.9%, 48.5%, 56.4% of wind velocity reduction when the angle between the main street grid and the prevailing wind is 22.5° (WSW), 45° (SW) and 67.5° (SSW) respectively. Consequently, volumetric average MAA at the street-level is the smallest under W wind at 38.1. The value increases to 48.0 (25.9% increase), 50.4 (32.1% increase), 65.8 (72.7% increase) as the incoming wind changes by 22.5° (WSW), 45° (SW) and 67.5° (SSW) respectively. Since the street grids are difficult to be modified remarkably for the existing metropolitan area of Hong Kong and many other urban environments, the variation of site types and tower form becomes another important factor that affects the pedestrian wind flow.

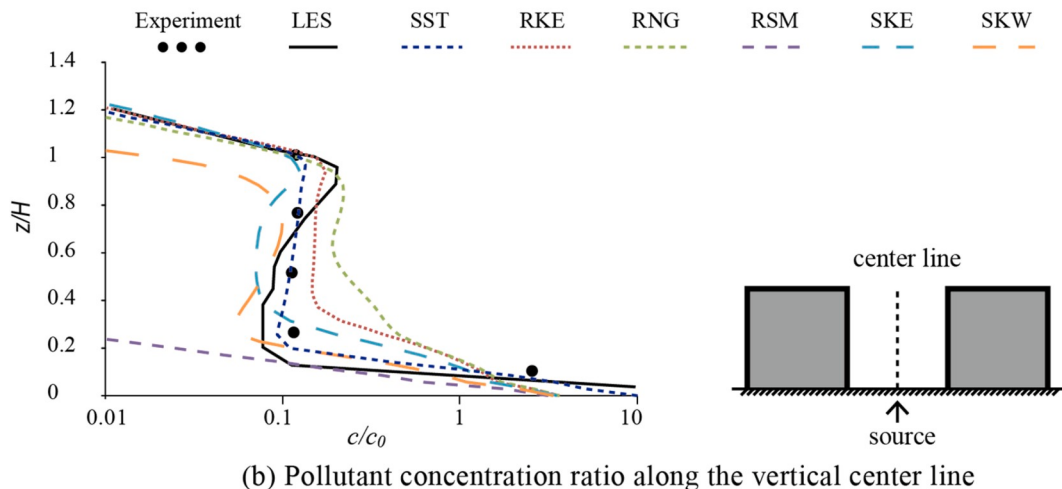
The result shows that extra-large sites have the potential to provide better street-level ventilation, which is highly influenced by the tower types. Among all the cases, S_{4000-3} has the best street-level ventilation performance under most of the wind directions with the largest average WVR at 0.36 and the smallest average MAA at 40. On the contrary, S_{4000-1} and S_{4000-2} , sharing the same site division strategies with S_{4000-3} , but has poor street-level ventilation. The large site such as S_{2000b} and S_{2000a} also provide better street-level ventilation by having the second and third smallest average MAA.

On the other hand, small and medium sites tend to have worse street-level ventilation. S_{1000b} has the worst street-level ventilation performance with the highest volumetric average MAA at 66 and the second smallest average WVR at 0.27. While S_{500b} has the smallest average WVR at 0.24 and second biggest MAA at 56. It seems that adopting irregular and unaligned tower shapes for small sites would harm the street-level ventilation. It is noticeable that S_{1000b} has the highest MAA under SSW wind, although its WVR is not the smallest. This can be explained by the unaligned arrangement and the irregular shape of towers, and also the large distance between tower and podium boundary facing the wind direction. This feature causes more airflow distortion and recirculation that keeps the momentum of incoming wind while failing to dissipate the aged air efficiently.

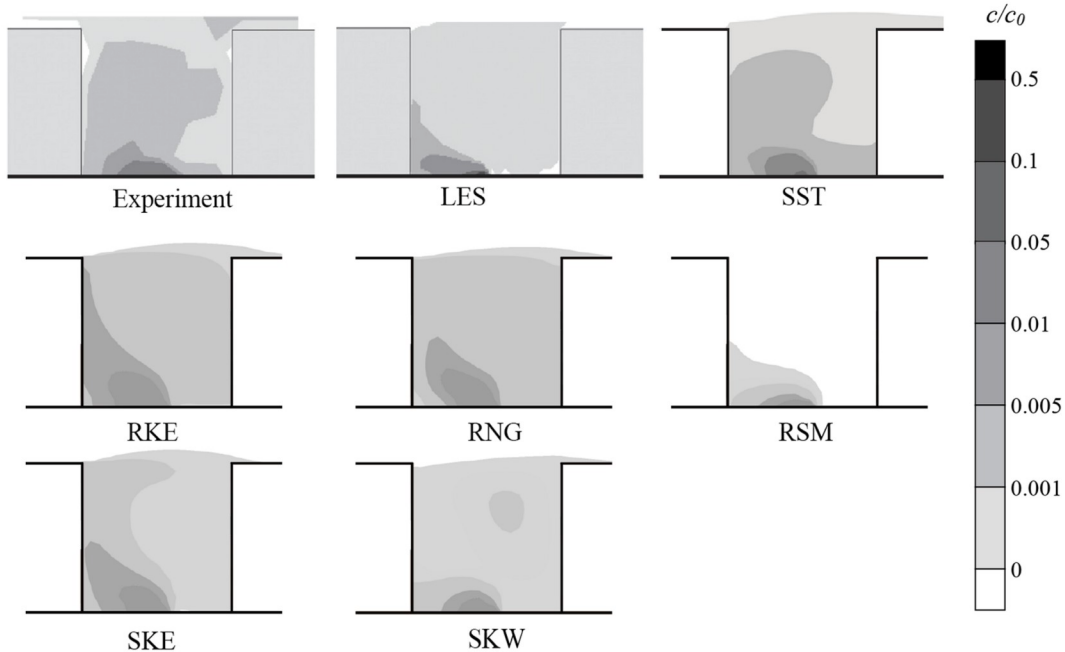
On the other hand, the provision of service lane for the cases with small site division strategies can help to significantly improve their street-level ventilation. Compared to S_{500b} , S_{500a} has a larger WVR at 0.30 (25% improvement) and smaller MAA at 50 (11% improvement). Similarly, S_{1000a} has 19% higher WVR and 29% lower MAA than S_{1000b} , while S_{2000a} has 7% higher WVR and 1% lower MAA compared to S_{2000b} .



(a) wind velocity ratio



(b) Pollutant concentration ratio along the vertical centerline



(c) Pollutant concentration ratio distribution inside the street canyon

Fig. 8. (a) Wind velocity ratio along the centerline from pollutant source to the street canyon top; Pollutant concentration ratio distribution (b) along the vertical centerline and (c) in the street canyon.

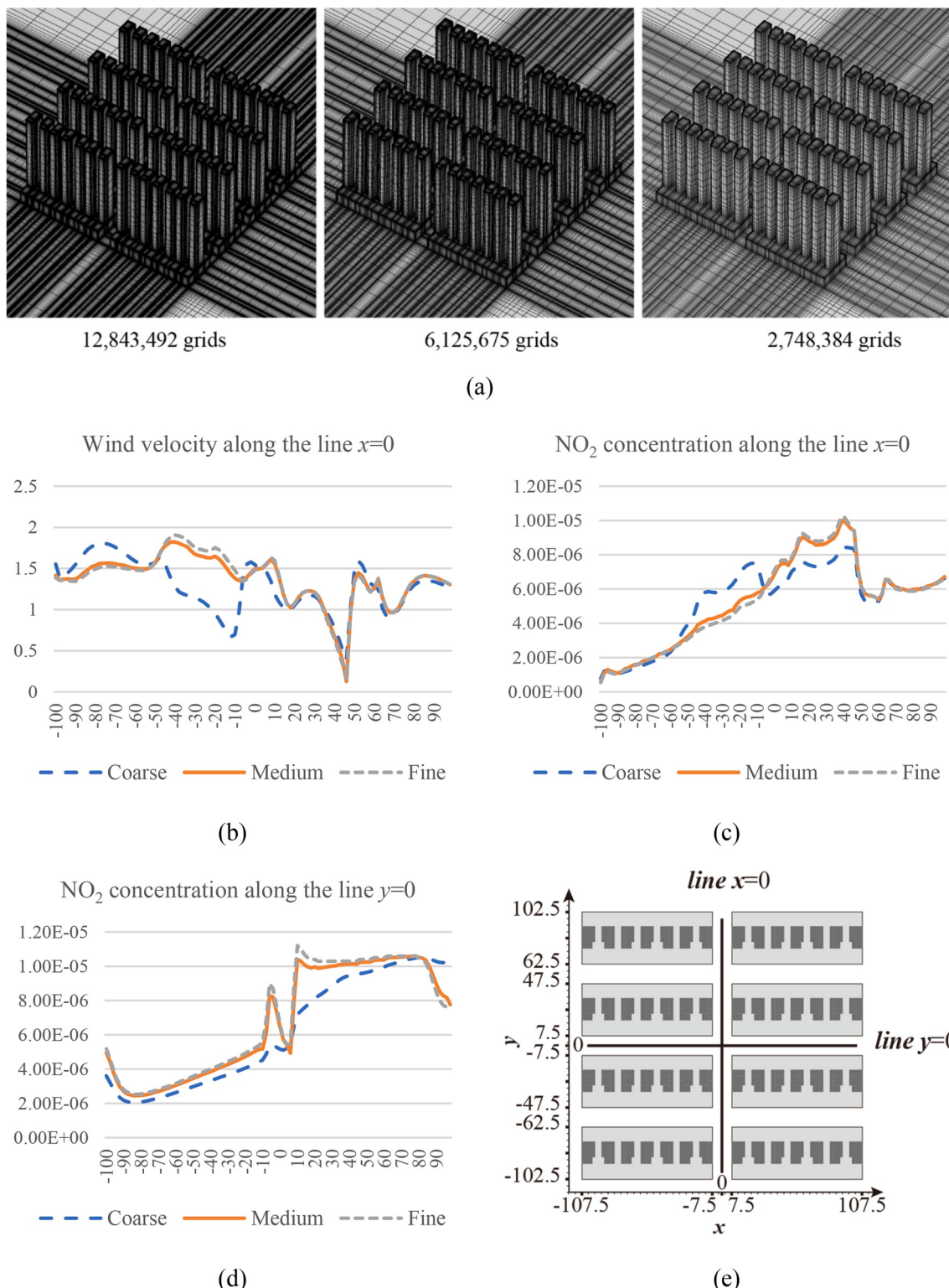


Fig. 9. Grid sensitivity analysis with (a) grid size of each cases, (b) Wind velocity along the line $x = 0$, (c) NO₂ concentration along the line $x = 0$, (d) NO₂ concentration along the line $y = 0$, (e) location of line $x = 0$ and $y = 0$.

This may be explained by the fact that adding Service Lanes in S_{500a}, S_{1000a} and S_{2000a} helps to improve the permeability at the street-level. This finding can be further confirmed by the comparison between S_{2000a} and S₄₀₀₀₋₁. With similar tower shapes, the difference in the results of these two cases could help to eliminate the suspect that particular tower types may be the sole cause of the enhancement in the street-level ventilation. It is found that S_{2000a} can improve WVR by 7% and

reduce MAA by 17%, compared to S₄₀₀₀₋₁. However, it should also be noticed that due to the different tower typologies, the impact of providing Service Lanes on increasing the ventilation varies.

5.2. Ventilation performance at the tower-level

Tower-level ventilation shows the ventilation performance between

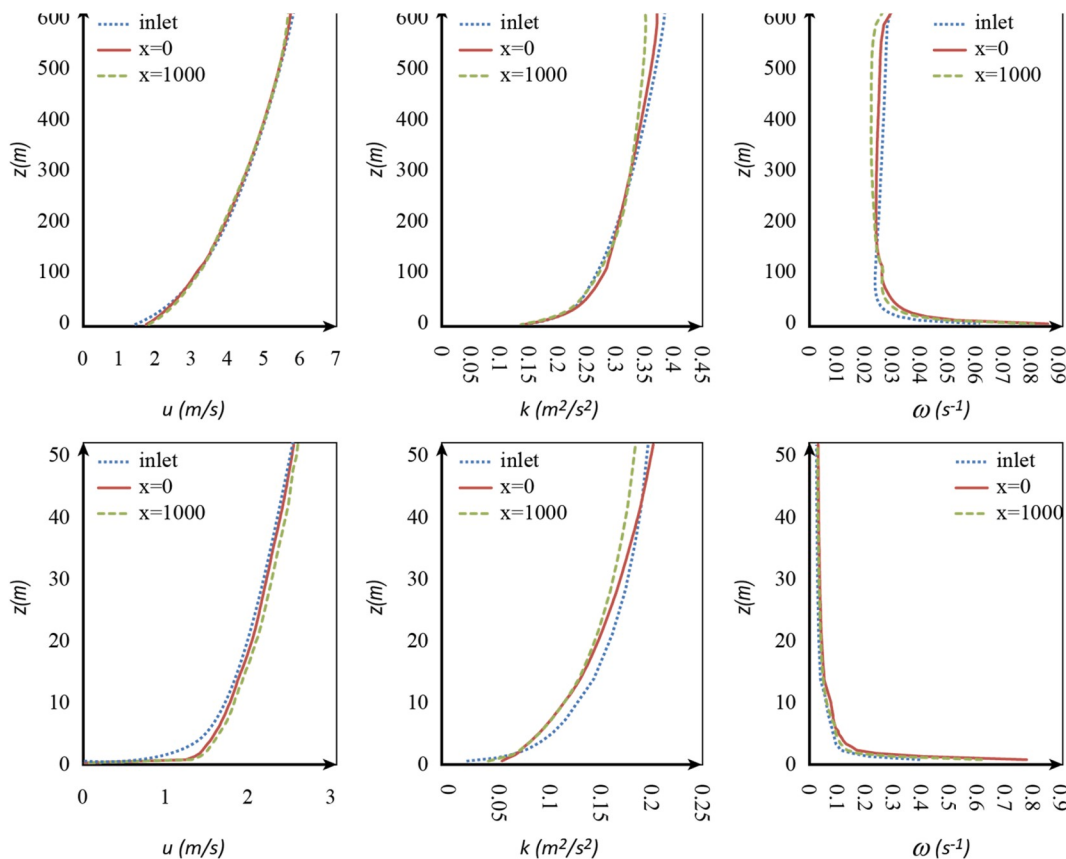


Fig. 10. Comparison between inlet and incident flow profiles, the top row shows the lowest 600 m of the boundary layer; the bottom row shows the lowest 50 m.

15 and 111 m. The distribution of age of air at 49.5 m above the ground, the volumetric average MAA at the tower-level, and average MAA at the tower façade of each case under four wind directions are summarized in Fig. 12. Average MAA at the tower façade is calculated by averaging the Age of air value at all the tower façade. This value is presented because air quality near the towers is important to the health of the residents living in the towers.

Similar to the street-level ventilation, the MAA at the tower-level increases when the angle between the main street grid and the prevailing wind rises. The average MAA of all 9 cases is 74 under W wind, 93 under WSW wind, 110 under SW wind and 126 under SSW wind, meaning there will be 25.3%, 48.1%, 69.0% of MAA increase when the angle between the main street grid and the prevailing wind is 22.5°, 45° and 67.5° respectively.

As shown in Fig. 12b, S_{500a} and S_{1000b} have the largest average MAA at 118 (100%), followed by S_{1000a} at 106 (10% improvement), S_{2000a} at 99 (16% improvement), S₄₀₀₀₋₂ and S_{2000b} at 96 (19% improvement), S₄₀₀₀₋₃ at 94 (20% improvement), S_{500b} at 92 (22% improvement) and S₄₀₀₀₋₁ at 89 (25% improvement). The result demonstrates that the extra-large sites (S₄₀₀₀) with centralized tower plans can provide better urban ventilation, while large sites (S₂₀₀₀) has moderate tower-level ventilation and the small sites (S₁₀₀₀ and S₅₀₀) tend to have poor tower-level ventilation. Exceptionally, S_{500b} adopts small site division strategies but still has the second smallest volumetric average MAA at 92.0. It shows that by choosing regular rectangular tower shapes and placing one row of towers along the windward direction, small sites could be able to provide better urban ventilation.

Since tower-level ventilation not only reflects the urban ventilation performance but also the potential of providing better indoor natural ventilation performance, the average MAA at the tower façade is summarized in Fig. 12c. It represents the freshness of open air that can be utilized by each residential tower for indoor natural ventilation. S₄₀₀₀₋₂

has the largest average MAA at tower façade at 148 due to its deep and irregular re-entrant, followed by S₄₀₀₀₋₁ at 143 (3% improvement), S_{2000a} at 136 (8% improvement), S_{1000a} at 135 (9% improvement), S_{500a} at 128 (14% improvement), S_{1000b} at 126 (15% improvement), S₄₀₀₀₋₃ at 124 (16% improvement) and S_{2000b} at 115 (22% improvement). S_{500b} has the best indoor air quality potential with the smallest average MAA at the tower façade at 107 (28% improvement). Overall, S_{500b} with small site division shows the best tower-level ventilation performance by getting second place in urban ventilation and the first place in indoor air quality potential. The result shows that the indoor natural ventilation potential is mainly affected by the tower plans. Small plans with the rectangular shape (S_{500b}) can provide the best indoor natural ventilation potential, followed by larger plans (S_{2000b}, S₄₀₀₀₋₃ and S_{1000a}), and then by small irregular tower plans (S_{500a}), and finally the plans with deep re-entrant (S_{1000b}, S_{2000a}, S₄₀₀₀₋₁ and S₄₀₀₀₋₂). The deeper the re-entrant is, the worse the indoor natural ventilation potential.

5.3. Discussion

For extra-large site types around 4000 square meters, they have the potential of providing better tower-level ventilation but tend to have poor indoor ventilation potential and unguaranteed street-level ventilation performance. S₄₀₀₀₋₃ has the best street-level ventilation performance and ranks third in the tower-level ventilation and indoor air quality potential. S₄₀₀₀₋₁ has the best tower-level ventilation, while not performing so well in the street-level ventilation and getting second last in the indoor air quality potential. S₄₀₀₀₋₂ has poor indoor air quality potential, street-level ventilation, and moderate tower-level ventilation. This can be explained by the fact that large centralized tower plans normally have a smaller frontal area, which benefits urban ventilation. But the deep re-entrants of these plans tend to cause indoor air quality problems. Therefore it is important to adopt a centralized tower plan

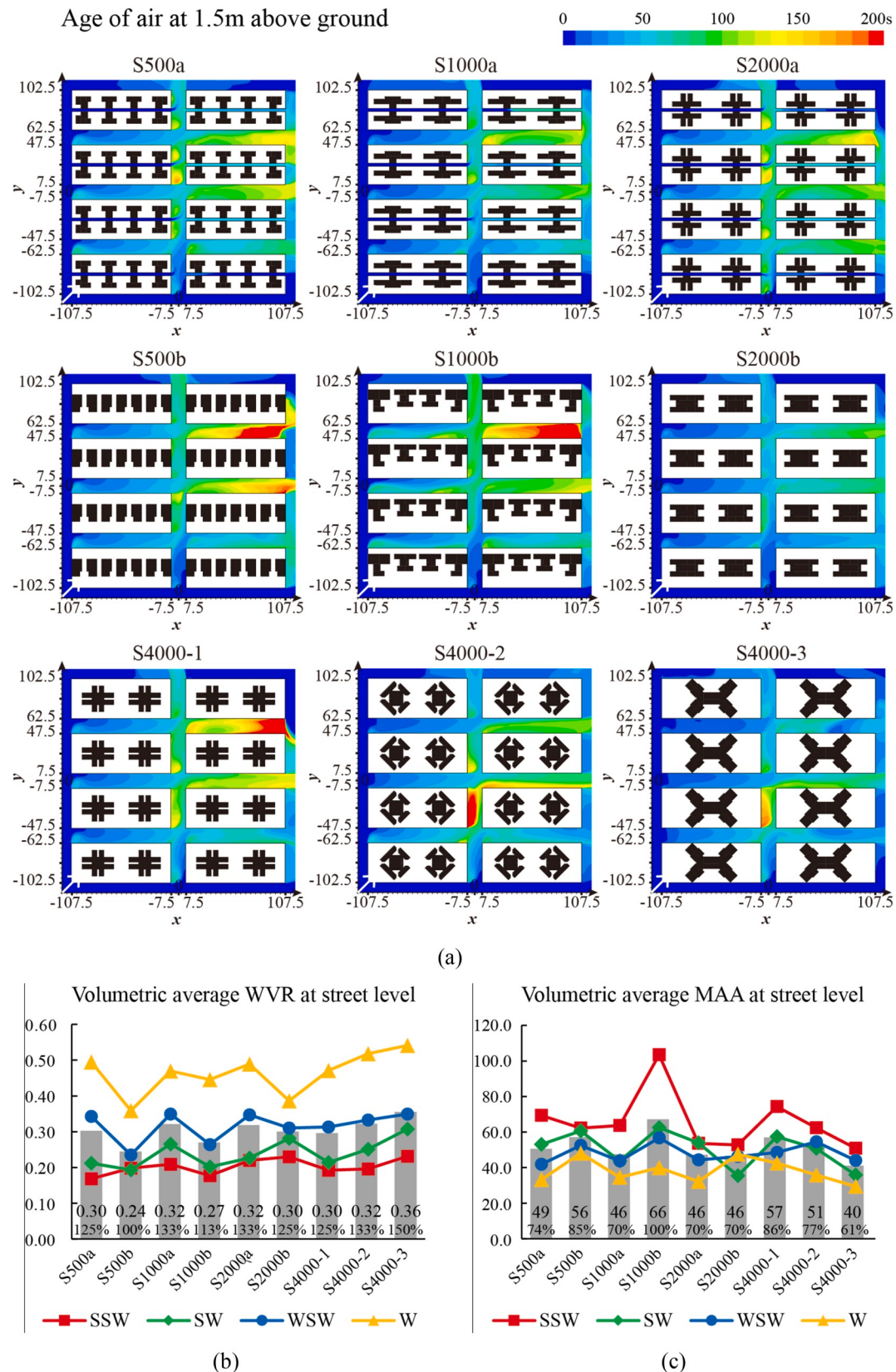


Fig. 11. (a) Distribution of age of air at 1.5 m above the ground under the SW incoming wind; (b) Volumetric average WVR at the street-level (m/s); (c) Volumetric average MAA at the street-level (s).

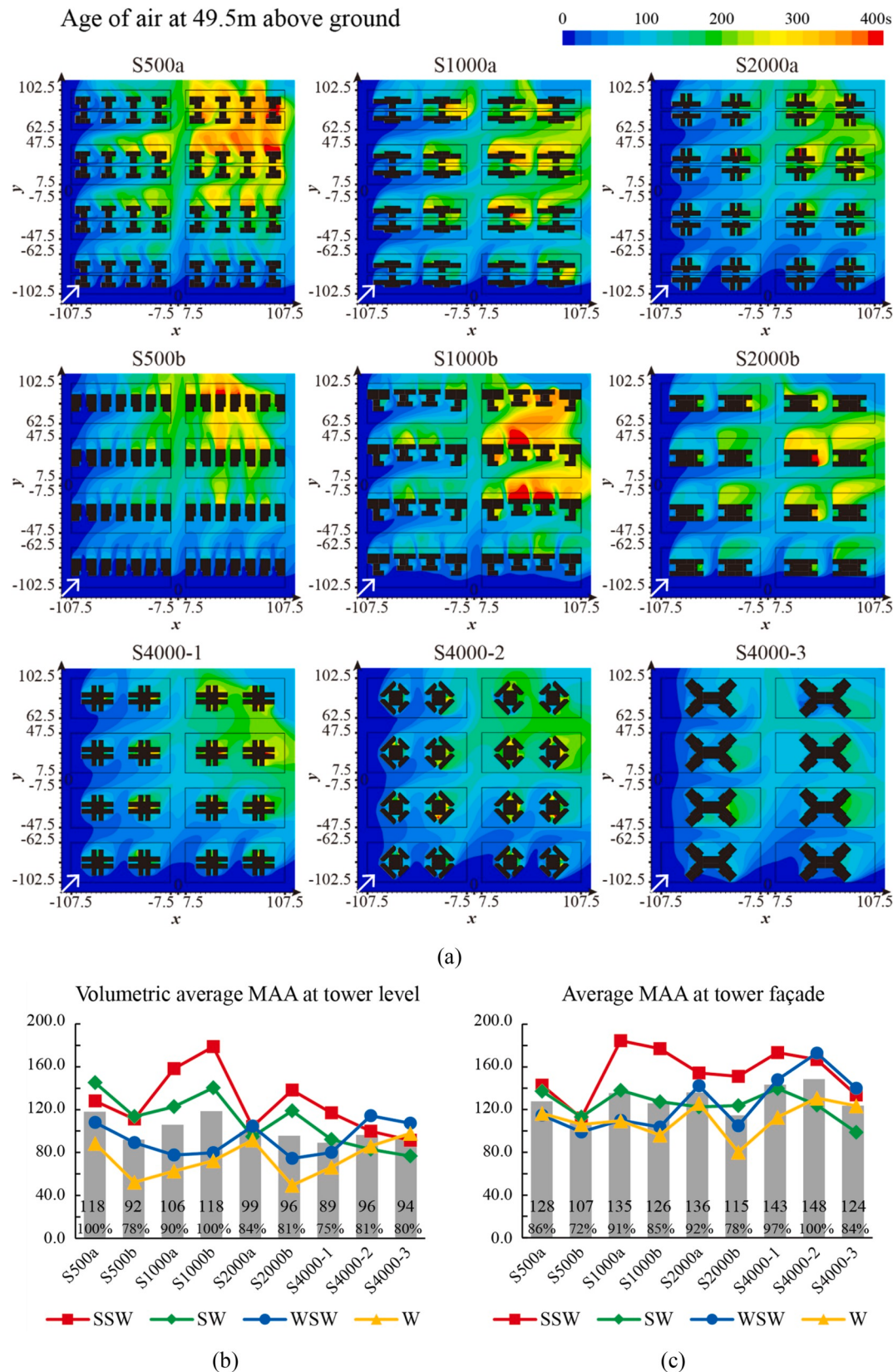


Fig. 12. (a) Distribution of age of air at 49.5 m above the ground under the SW incoming wind; (b) Volumetric average MAA at the tower-level; (c) Average MAA at the tower façade.

and meanwhile avoid deep re-entrants, such as S₄₀₀₀₋₃.

For small (around 500 square meters) and medium (around 1000 square meters) sites, providing service lane can help to improve street-level ventilation, while it tends to cause poor tower-level ventilation since there are two rows of towers in one street block. Examples would be S_{1000a} and S_{500a}, which rank fourth and fifth in the street-level ventilation respectively and rank third last and second last in the tower-level ventilation. For those small and medium sites that can not have service lanes, adopting small and rectangular floor plans and placing one row of towers along the long side would ensure good tower-level ventilation and best indoor air quality potential. The best example is S_{500b} which has the poorest street-level ventilation performance but the best indoor air quality potential and second best tower-level ventilation performance.

6. Conclusion

This paper investigates the urban ventilation performance at the street and tower-level in the high-rise high-density urban environment of Hong Kong through an innovative way of generating the urban forms. It is found that the selection of tower types is highly affected by the site type and site division strategies due to the “view optimization principle”. The impact of site division strategies and corresponding tower types on urban ventilation and indoor air quality potential were evaluated using CFD simulation. The following conclusions can be drawn:

- Street grids with more streets parallel to the prevailing wind direction can provide better urban ventilation.
- Extra-large site division strategies (S₄₀₀₀) have the potential of achieving the best performance in both street and tower-level ventilation. However, it also has the largest uncertainty on the street-level ventilation, since large sites offer the developers with much more freedom on the tower selection. Besides, since large centralized floor plans with deep re-entrants are usually adopted, it tends to cause poor indoor air quality potential. Therefore, it is important to develop urban design regulations and guidelines to advise the developers to choose more suitable tower types.
- Large site (S₂₀₀₀) with or without service lane can both provide good street-level ventilation and moderate tower-level ventilation. By choosing “H” shape plans with shallow re-entrant, it also has the potential in providing good indoor natural ventilation at the tower-level.
- Small (S₅₀₀) and medium (S₁₀₀₀) sites generally have poor street-level ventilation. Adopting irregular and unaligned tower shapes for small sites will further harm the street-level ventilation. On the other hand, for the small sites without service lanes, choosing towers with small rectangular plans in one row could help to achieve better tower-level ventilation and indoor air quality potential.
- Adding service lane can help to improve the street ventilation, but may cause poor tower-level ventilation since two rows of towers are closely placed in one street block.

Limitation and future study: The site and towers are studied from the typological aspect without inspection of detailed morphological factors. A detailed study with more variation on the podium and tower morphology considering the width, depth, aspect ratio, and shape factor will be conducted. Moreover, since different towers provide a different number of bedrooms that affects their ability in accommodating residents, how to optimize the social-economic benefits and urban ventilation will also be studied in the future.

Funding

This work was supported by Open Projects Fund (project number: 2019020113) of Shanghai Key Laboratory of Urban Renewal and Spatial Optimization Technology, Tongji University, Shanghai, China.

Declaration of competing interest

The authors declare that they have no known competing financial interests or personal relationships that could have appeared to influence the work reported in this paper.

References

- [1] B. Gurjar, L. Molina, C. Ojha, Air pollution: health and environmental concerns, in: *Air Pollut. Heal. Environ. Impacts*, 2010, pp. 1–15, <https://doi.org/10.1201/EBK1439809624>.
- [2] S.-K. Wong, L. Wai-Chung Lai, D.C.-W. Ho, K.-W. Chau, C. Lo-Kuen Lam, C. Hung-Fai Ng, Sick building syndrome and perceived indoor environmental quality: a survey of apartment buildings in Hong Kong, *Habitat Int.* 33 (2009) 463–471, <https://doi.org/10.1016/j.habitatint.2009.03.001>.
- [3] H. Lin, Q. An, C. Luo, V.C. Pun, C.S. Chan, L. Tian, Gaseous air pollution and acute myocardial infarction mortality in Hong Kong: a time-stratified case-crossover study, *Atmos. Environ.* 76 (2013) 68–73, <https://doi.org/10.1016/j.atmosenv.2012.08.043>.
- [4] W. Pan, H. Qin, Y. Zhao, Challenges for energy and carbon modeling of high-rise buildings: the case of public housing in Hong Kong, *Resour. Conserv. Recycl.* 123 (2017) 208–218, <https://doi.org/10.1016/j.resconrec.2016.02.013>.
- [5] H. Qin, W. Pan, Energy use of subtropical high-rise public residential buildings and impacts of energy saving measures, *J. Clean. Prod.* 254 (2020) 120041, <https://doi.org/10.1016/j.jclepro.2020.120041>.
- [6] L.W.C. Lai, D.C.W. Ho, K.W. Chau, M.H. Chua, Repeated planning applications by developers under statutory zoning: a Hong Kong case study of delays and design improvements in private residential development, *Land Use Pol.* 57 (2016) 709–718, <https://doi.org/10.1016/j.landusepol.2016.06.031>.
- [7] M. Skote, M. Sandberg, U. Westerberg, L. Claesson, a Johansson, Numerical and experimental studies of wind environment in an urban morphology, *Atmos. Environ.* 39 (2005) 6147–6158, <https://doi.org/10.1016/j.atmosenv.2005.06.052>.
- [8] J. Hang, Y. Li, Ventilation strategy and air change rates in idealized high-rise compact urban areas, *Build. Environ.* 45 (2010) 2754–2767, <https://doi.org/10.1016/j.buildenv.2010.06.004>.
- [9] Y. Tominaga, T. Stathopoulos, CFD modeling of pollution dispersion in a street canyon: comparison between LES and RANS, *J. Wind Eng. Ind. Aerod.* 99 (2011) 340–348, <https://doi.org/10.1016/j.jweia.2010.12.005>.
- [10] O.S. Asfour, M.B. Gadi, A comparison between CFD and Network models for predicting wind-driven ventilation in buildings, *Build. Environ.* 42 (2007) 4079–4085, <https://doi.org/10.1016/j.buildenv.2006.11.021>.
- [11] B. Blocken, T. Stathopoulos, P. Saathoff, X. Wang, Numerical evaluation of pollutant dispersion in the built environment: comparisons between models and experiments, *J. Wind Eng. Ind. Aerod.* 96 (2008) 1817–1831, <https://doi.org/10.1016/j.jweia.2008.02.049>.
- [12] M. Shirzadi, M. Naghashzadegan, P.A. Mirzaei, Improving the CFD modelling of cross-ventilation in highly-packed urban areas, *Sustain. Cities Soc.* 37 (2018) 451–465, <https://doi.org/10.1016/j.scs.2017.11.020>.
- [13] Y.F. Lun, A. Mochida, S. Murakami, H. Yoshino, T. Shirasawa, Numerical simulation of flow over topographic features by revised k-e models, *J. Wind Eng. Ind. Aerod.* 91 (2003) 231–245, [https://doi.org/10.1016/S0167-6105\(02\)00348-3](https://doi.org/10.1016/S0167-6105(02)00348-3).
- [14] Y. Tominaga, T. Stathopoulos, Numerical simulation of dispersion around an isolated cubic building: comparison of various types of k-e models, *Atmos. Environ.* 43 (2009) 3200–3210, <https://doi.org/10.1016/j.atmosenv.2009.03.038>.
- [15] J.I. Perén, T. van Hooff, B.C.C. Leite, B. Blocken, CFD analysis of cross-ventilation of a generic isolated building with asymmetric opening positions: impact of roof angle and opening location, *Build. Environ.* 85 (2015) 263–276, <https://doi.org/10.1016/j.buildenv.2014.12.007>.
- [16] Y. Topalar, B. Blocken, B. Maihue, G.J.F. van Heijst, A review on the CFD analysis of urban microclimates, *Renew. Sustain. Energy Rev.* 80 (2017) 1613–1640, <https://doi.org/10.1016/j.rser.2017.05.248>.
- [17] Z. Tong, Y. Chen, A. Malkawi, Defining the Influence Region in neighborhood-scale CFD simulations for natural ventilation design, *Appl. Energy* 182 (2016) 625–633, <https://doi.org/10.1016/j.apenergy.2016.08.098>.
- [18] R. Ramponi, B. Blocken, CFD simulation of cross-ventilation for a generic isolated building: impact of computational parameters, *Build. Environ.* 53 (2012) 34–48, <https://doi.org/10.1016/j.buildenv.2012.01.004>.
- [19] J. Franke, A. Hellsten, H. Schlünzen, B. Carissimo, K.H. Schlünzen, B. Carissimo, H. Schlünzen, The COST 732 Best Practice Guideline for CFD simulation of flows in the urban environment: a summary, *Int. J. Environ. Pollut.* 44 (2011) 419–427, <https://doi.org/10.1504/IJEP.2011.038443>.
- [20] Y. Li, T. Stathopoulos, Numerical evaluation of wind-induced dispersion of pollutants around a building, *J. Wind Eng. Ind. Aerod.* (1997) 67–68, [https://doi.org/10.1016/S0167-6105\(97\)00116-5](https://doi.org/10.1016/S0167-6105(97)00116-5), 757–766.
- [21] K. Zhang, G. Chen, X. Wang, S. Liu, C.M. Mak, Y. Fan, J. Hang, Numerical evaluations of urban design technique to reduce vehicular personal intake fraction in deep street canyons, *Sci. Total Environ.* 653 (2019) 968–994, <https://doi.org/10.1016/j.scitotenv.2018.10.333>.
- [22] J. Hang, Z. Xian, D. Wang, C.M. Mak, B. Wang, Y. Fan, The impacts of viaduct settings and street aspect ratios on personal intake fraction in three-dimensional urban-like geometries, *Build. Environ.* 143 (2018) 138–162, <https://doi.org/10.1016/j.buildenv.2018.07.001>.

- [23] S.H.L.H.L. Yim, J.C.H.C.H. Fung, a.K.H.K.H. Lau, S.C.C. Kot, Air ventilation impacts of the “wall effect” resulting from the alignment of high-rise buildings, *Atmos. Environ.* 43 (2009) 4982–4994, <https://doi.org/10.1016/j.atmosenv.2009.07.002>.
- [24] C. Ding, K.P. Lam, Data-driven model for cross ventilation potential in high-density cities based on coupled CFD simulation and machine learning, *Build. Environ.* 165 (2019) 106394, <https://doi.org/10.1016/j.buildenv.2019.106394>.
- [25] L. Chen, J. Hang, M. Sandberg, L. Claesson, S. Di Sabatino, H. Wigo, The impacts of building height variations and building packing densities on flow adjustment and city breathability in idealized urban models, *Build. Environ.* 118 (2017) 344–361, <https://doi.org/10.1016/j.buildenv.2017.03.042>.
- [26] J. Allegrini, V. Dorer, J. Carmeliet, Buoyant flows in street canyons: validation of CFD simulations with wind tunnel measurements, *Build. Environ.* 72 (2014) 63–74, <https://doi.org/10.1016/j.buildenv.2013.10.021>.
- [27] J. Hang, Z. Luo, X. Wang, L. He, B. Wang, W. Zhu, The influence of street layouts and viaduct settings on daily carbon monoxide exposure and intake fraction in idealized urban canyons, *Environ. Pollut.* 220 (2017) 72–86, <https://doi.org/10.1016/j.envpol.2016.09.024>.
- [28] J. Allegrini, V. Dorer, J. Carmeliet, Influence of morphologies on the microclimate in urban neighbourhoods, *J. Wind Eng. Ind. Aerod.* 144 (2015) 108–117, <https://doi.org/10.1016/j.jweia.2015.03.024>.
- [29] B. Blocken, J. Persoon, Pedestrian wind comfort around a large football stadium in an urban environment: CFD simulation, validation and application of the new Dutch wind nuisance standard, *J. Wind Eng. Ind. Aerod.* 97 (2009) 255–270, <https://doi.org/10.1016/j.jweia.2009.06.007>.
- [30] N. Antoniou, H. Montazeri, H. Wigo, M.K.A. Neophytou, B. Blocken, M. Sandberg, CFD and wind-tunnel analysis of outdoor ventilation in a real compact heterogeneous urban area: evaluation using “air delay”, *Build. Environ.* 126 (2017) 355–372, <https://doi.org/10.1016/j.buildenv.2017.10.013>.
- [31] B. Blocken, W.D.D. Janssen, T. van Hooff, CFD simulation for pedestrian wind comfort and wind safety in urban areas: general decision framework and case study for the Eindhoven University campus, *Environ. Model. Software* 30 (2012) 15–34, <https://doi.org/10.1016/j.envsoft.2011.11.009>.
- [32] C. Yuan, E. Ng, Building porosity for better urban ventilation in high-density cities – a computational parametric study, *Build. Environ.* 50 (2012) 176–189, <https://doi.org/10.1016/j.buildenv.2011.10.023>.
- [33] Y. He, A. Tablada, N.H. Wong, A parametric study of angular road patterns on pedestrian ventilation in high-density urban areas, *Build. Environ.* 151 (2019) 251–267, <https://doi.org/10.1016/j.buildenv.2019.01.047>.
- [34] HKPD, Hong Kong geographic data. <http://www.landsd.gov.hk/mapping/en/publications/map.htm>, 2010.
- [35] P.D. HKSAR, Broad Land Usage Distribution, 2010. http://www.pland.gov.hk/pland_en/info_serv/statistic/landu.html.
- [36] HKCSD, Hong Kong annual digest of statistics, 2014. Hong Kong.
- [37] P. Lin, S.S.Y. Lau, H. Qin, Z. Gou, Effects of urban planning indicators on urban heat island: a case study of pocket parks in high-rise high-density environment, *Landsc. Urban Plann.* 168 (2017) 48–60. <https://www.sciencedirect.com/science/article/pii/S0169204617302554>. accessed October 27, 2017.
- [38] HKBD/HKSAR, Building (Planning) Regulations 2012, Historical Laws of Hong Kong Online, Hong Kong, 2012. <http://oelawhk.lib.hku.hk/items/show/2542>.
- [39] A. Sharifi, Resilient urban forms: a review of literature on streets and street networks, *Build. Environ.* 147 (2019) 171–187, <https://doi.org/10.1016/j.buildenv.2018.09.040>.
- [40] C.Q.L. Xue, H. Zou, B. Li, K.C. Hui, The shaping of early Hong Kong: transplantation and adaptation by the British professionals, 1841–1941, *Plann. Perspect.* 27 (2012) 549–568, <https://doi.org/10.1080/02665433.2012.705124>.
- [41] H.K. HKPD, Planning Standards & Guidelines-Residential Densities, 2016.
- [42] C.Y. Jim, W.Y. Chen, Value of scenic views: hedonic assessment of private housing in Hong Kong, *Landsc. Urban Plann.* 91 (2009) 226–234, <https://doi.org/10.1016/j.landurbplan.2009.01.009>.
- [43] HKBD, APP-73: service lanes, 1995.
- [44] J. Franke, Recommendations of the COST action C14 on the use of CFD in predicting pedestrian wind environment, *Fourth Int. Symp. Comput. Wind Eng.* (2006) 529–532.
- [45] Y. Tominaga, A. Mochida, R. Yoshie, H. Kataoka, T. Nozu, M. Yoshikawa, T. Shirasawa, AJ guidelines for practical applications of CFD to pedestrian wind environment around buildings, *J. Wind Eng. Ind. Aerod.* 96 (2008) 1749–1761, <https://doi.org/10.1016/j.jweia.2008.02.058>.
- [46] HKSAR, Air ventilation assessments, 2006. Hong Kong.
- [47] HKPD, CUHK, Experimental Site Wind Availability Study for Mong Kok, Hong Kong, The Chinese University of Hong Kong, Hong Kong, 2008.
- [48] AJ, Wind loads, AJ Recom., Loads Build., 2004.
- [49] J. Hang, Y. Li, Wind Conditions and City Ventilation in Idealized City Models, The University of Hong Kong, 2009.
- [50] J. Hang, Y. Li, Age of air and air exchange efficiency in high-rise urban areas and its link to pollutant dilution, *Atmos. Environ.* 45 (2011) 5572–5585, <https://doi.org/10.1016/j.atmosenv.2011.04.051>.
- [51] B.E. Launder, D.B. Spalding, *Lectures in Mathematical Models of Turbulence*, Academic Press, London, 1972.
- [52] T.-H. Shih, W.W. Liou, A. Shabbir, Z. Yang, J. Zhu, A new k- ϵ eddy viscosity model for high Reynolds number turbulent flows, *Comput. Fluid* 24 (1995) 227–238, [https://doi.org/10.1016/0045-7930\(94\)00032-t](https://doi.org/10.1016/0045-7930(94)00032-t).
- [53] V. Yakhot, S.A. Orszag, Renormalization group analysis of turbulence. I. Basic theory, *J. Sci. Comput.* 1 (1986) 3–51, <https://doi.org/10.1007/bf01061452>.
- [54] D.C. Wilcox, *Turbulence Modeling for CFD*, second ed., DCW Industries, La Canada, Calif., 1998.
- [55] F.R. Menter, Two-equation eddy-viscosity turbulence models for engineering applications, *AIAA J.* (1994) 1598–1605, <https://doi.org/10.5594/smpte.rp2079.2017>.
- [56] B.E. Launder, Second-moment closure: present... and future? *Int. J. Heat Fluid Flow* 10 (1989) 282–300, [https://doi.org/10.1016/0142-727x\(89\)90017-9](https://doi.org/10.1016/0142-727x(89)90017-9).
- [57] Y. Tominaga, T. Stathopoulos, CFD Modeling of Pollution Dispersion in Building Array: evaluation of turbulent scalar flux modeling in RANS model using LES results, *J. Wind Eng. Ind. Aerodyn.* 104–106 (2012) 484–491, <https://doi.org/10.1016/j.jweia.2012.02.004>.
- [58] T. van Hooff, B. Blocken, Coupled urban wind flow and indoor natural ventilation modelling on a high-resolution grid: a case study for the Amsterdam ArenA stadium, *Environ. Model. Software* 25 (2010) 51–65, <https://doi.org/10.1016/j.envsoft.2009.07.008>.
- [59] B. Blocken, T. Stathopoulos, J. Carmeliet, CFD simulation of the atmospheric boundary layer: wall function problems, *Atmos. Environ.* 41 (2007) 238–252, <https://doi.org/10.1016/j.atmosenv.2006.08.019>.
- [60] B. Blocken, J. Carmeliet, T. Stathopoulos, CFD evaluation of wind speed conditions in passages between parallel buildings—effect of wall-function roughness modifications for the atmospheric boundary layer flow, *J. Wind Eng. Ind. Aerod.* 95 (2007) 941–962, <https://doi.org/10.1016/j.jweia.2007.01.013>.
- [61] H. Yu, J. Thé, Validation and optimization of SST k- ω turbulence model for pollutant dispersion within a building array, *Atmos. Environ.* 145 (2016) 225–238, <https://doi.org/10.1016/j.atmosenv.2016.09.043>.